ESTIMATING A GREEN'S FUNCTION FROM "FIELD-FIELD" CORRELATIONS IN A RANDOM MEDIUM*

MAARTEN V. DE HOOP† AND KNUT SOLNA‡

Abstract. Traditional imaging methods use coherent signals as data. Here, we discuss recent developments in imaging that aim at exploiting as data incoherent noisy signals that are not associated with well-defined arrival times. Indeed, signal constituents that in a classical setting may be regarded as noise may contain important information about the medium to be imaged. We show how it is possible to use the statistics of such noisy signals, specifically, the second-order statistics, for imaging. We consider two particular situations: first, the estimation of an ("empirical") Green's function from noisy signals which can subsequently be used in imaging; second, the localization of a cluster of random sources from noisy signals (passive imaging). The analysis presented here is based on assuming a remote sensing scaling and the paraxial approximation, and it uses in part the results set forth in Papanicolaou, Ryzhik, and Solna [*SIAM J. Appl. Math.*, 64 (2004), pp. 1133–1155] that relate to time-reversal, statistical stability, and superresolution. Robustness with respect to modeling assumptions is illustrated by considering other scaling regimes also. We demonstrate how the estimation problem and its robustness can be considered as a dual to that of time-reversal and stable superresolution. We obtain a novel analysis and foundation for the use of ambient seismic noise in body-wave (tomographic) imaging, motivated by the recent successes of surface-wave tomography using ambient seismic noise.

Key words. empirical Green's function, random medium, paraxial approximation, statistical stability

AMS subject classifications. 34F05, 34E10, 37H10, 60H20

DOI. 10.1137/070701790

1. Introduction.

1.1. Time-reversal and cross-correlation–based imaging. Recent work on time-reversal of waves in a random medium has shown that medium fluctuations are not necessarily detrimental to, but may in fact enhance various operations with, waves. This has been analyzed mathematically as well as demonstrated experimentally [4, 20, 22, 25, 30, 31, 33]. In classical time-reversal, the wave received by an active transducer (receiver-emitter) array is recorded and then re-emitted into the configuration time-reversed; that is, the tails of the recorded signals are sent first. In the absence of absorption, the re-emitted signal will propagate back toward the source and focus, approximately, on it. This phenomenon has a large number of applications, in inverse problems, medical imaging, remote sensing, target identification, and secure communication, for instance. Here, we discuss the notion of "field-field" cross-correlations associated with noise observed at pairwise distinct receivers, to obtain an "empirical" Green's function. This notion is naturally related to the time-reversal mentioned above [13, 14]. We will give a precise characterization of the "empirical" Green's function, which can subsequently be used for imaging the interrogated

medium. To this end, we consider a configuration consisting of a randomly heterogeneous halfspace, possibly containing a scatterer, which is exposed to random *noisy sources* concentrated at the surface (that is, the top of the halfspace). The idea is to use *cross-correlations* between a set of measurements of noise to infer information about the medium in the halfspace as well as about the location of the scatterer.

With seismology as a key application in mind, the goal is to obtain an image of Earth's interior from all possible signals recorded at an array of receiver stations. Robust imaging requires, essentially, a regular distribution of sources. Effectively using receivers as sources through the mentioned "field-field" cross-correlations, this requirement can be satisfied, even where deterministic sources (earthquakes) are necessarily absent. The idea of using ambient noise for the retrieval of a body-wave reflection response, in a planarly layered medium, dates back to Claerbout [8]. He also conjectured that, in general media, cross-correlating ambient noise traces from two locations recaptures the wavefield at one of the locations, excited by a point source at the other location. An early example of a field application was reported by Scherbaum [37], who analyzed auto-correlations of recordings of low-magnitude earthquakes and generated *pseudoreflection seismograms*. Moreover, the cross-correlation method has been developed in helioseismology [16]. In recent years, the understanding of how cross-correlating diffuse fields recaptures the Green's function has been a topic of research [46, 42]. Cross-correlating (diffuse) coda waves [7] and ambient seismic noise [38, 39] resulted in the retrieval of surface waves observed at one station and excited at the other station; for a detailed study, see Yao, van der Hilst, and deHoop [43]. Furthermore, *turning* body waves have been observed in cross-correlating ambient noise [35]; in an exploration seismology setting, *reflected* body waves have also been recovered by cross-correlations [15]. The exploitation of a scattering medium in capturing the Green's function by field-field cross-correlations was studied by Derode et al. [14]. The mathematical analysis of field-field cross-correlations in the mentioned setting from the point of view of heterogeneous media has just begun. See [26] for analysis of the case with a layered random medium and [3] for a recent analysis based on the semiclassical approximation and that explicitly discusses stability of the traveltime estimates associated with the correlations which requires a careful analysis of the time scales involved. In [10], field-field cross-correlations from ambient noise, which is not necessarily localized or directional, are analyzed in the high-frequency limit, again making use of Egorov's theorem of microlocal analysis. Here, motivated by applications to propagation in the heterogeneous earth and the atmosphere, we will consider the far field regime and consider a stochastic modeling approach. We exploit the random fluctuations in the medium and consider a variety of (scaling) regimes. In the above, noisy sources are passive sources, while the medium is subjected to random fluctuations. Controlled sources can be used to retrieve the Green's function from cross-correlations of wavefields observed at pairwise distinct receivers as well. Time-reversal and Rayleigh's reciprocity relation can be combined to easily identify the cross-correlation as the Green's function in the interior of a compact domain with controlled sources (everywhere) on its boundary without knowledge of the (deterministic) medium [12]; applications of this general result in borehole seismic imaging can be found in [28, 47, 44]. Insights in extending this situation to the case with decorrelating random sources (on the boundary) can be found, for example, in [45].

A proper estimate of the Green's function between a set of locations can be used for robust imaging from ambient noise [27, 39, 43] and for encoding signals also. The technique of cross-correlations is furthermore relevant in the context of
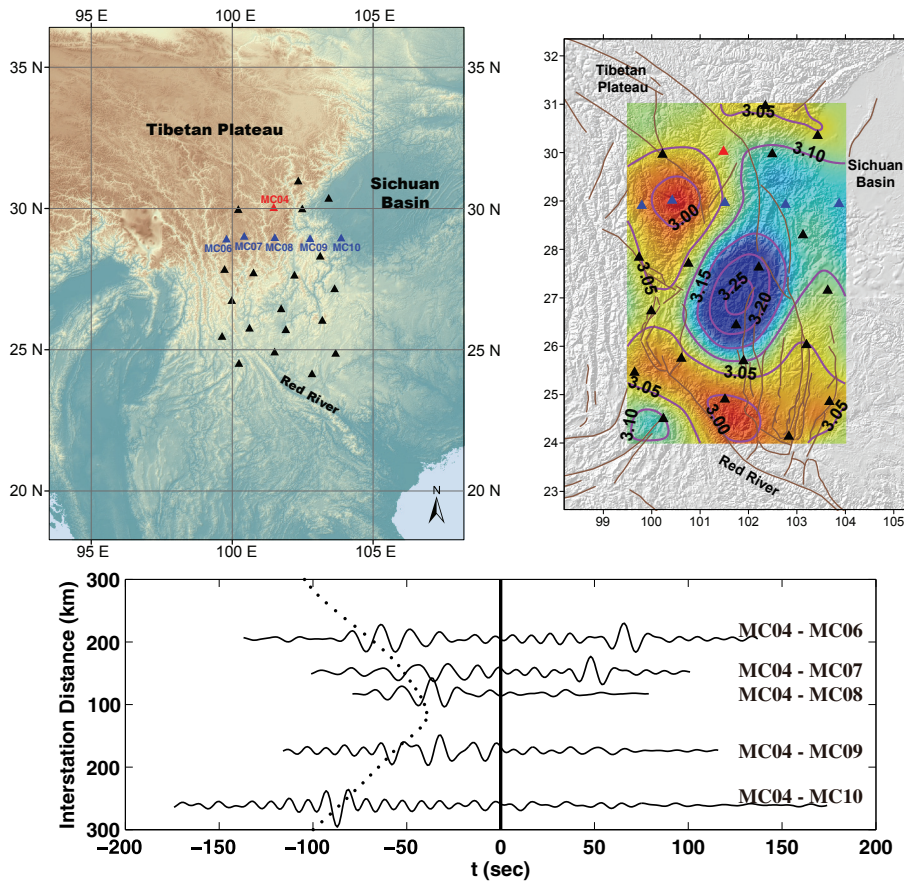
FIG. 1.1. *Top left: a map and the array of receivers. Top right: phase velocities at $T = 10\,s$ (obtained from the Green's function estimates between all pairs of receivers, and given in [43]); these phase velocities play the role of c_0. Bottom: Green's function estimates from 10 months of data cross-correlations. The positive times correspond to the Green's function from the "source" station $MC04$ (red) to receivers $MC**$ (blue), while the negative times correspond to the Green's function from the "source" stations $MC**$ (blue) to receiver station $MC04$ (red). We observe an asymmetry (in time) that will appear in the analysis presented here also. The dotted line indicates the traveltimes computed from the top right figure.*

communication in a waveguide [36] and synchronization of transducer array elements. Detection based on cross-correlations in a noisy environment is discussed in [1] and interferometric imaging in [6]. The theory for analysis of cross-correlations in layered media is presented in [25] with applications presented in, for instance, [23, 24]. While current studies relating to the heterogeneous earth mostly make use of surface-wave contributions to the Green's function estimate, we emphasize, here, the importance of understanding the behavior of body waves for future applications. In Figure 1.1 we illustrate surface-wave contributions to the Green's function estimate over an array in Southeastern Tibet (obtained from [43], upon cross-correlating noise between receiver pairs over a 10 month period).

In this paper, we analyze *estimation based on incoherent waves* in the context of the paraxial approximation and the associated Wigner distribution. We prove that,
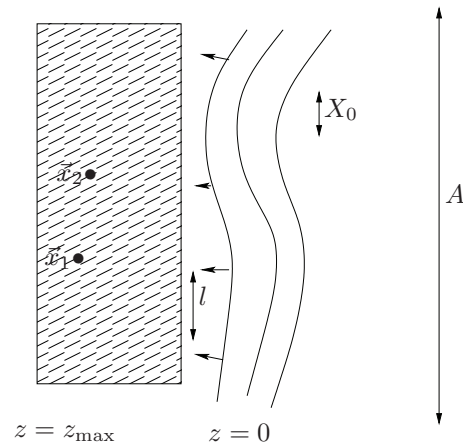
Fig. 1.2. *The experimental setup: A slab of random medium is located in $(0, z_{\max})$. In the plane $z = 0$ a set of random sources probe the medium, and we record the signal transmitted to the two points of observation $\vec{x}_1$ and $\vec{x}_2$.*

in principle, the Green's function can be recovered from cross-correlations, up to a filter that depends only mildly on the medium realization. Moreover, we show that much better estimates (when the Green's function is better resolved) may be obtained in a randomly inhomogeneous medium than in a deterministic (quasi-)homogeneous medium, as a consequence of the wider angular spread in the phase-space representation of a wave in the random medium; this is in agreement with the results of the experiment described in [13]. The enhanced resolution occurs due to an exponential damping factor that appears in the analysis of the cross-correlation and that involves the structure function of the medium; thus, relatively strong disorder gives relatively high resolution. The damping factor was also responsible for superresolution in the time-reversal experiment elucidated in [33], revealing an intrinsic connection. It appears to be important that the signals generating the cross-correlations are subjected to frequency-bandlimitation: The low frequencies must be removed to obtain accurate estimates.

Furthermore, we discuss the localization of a cluster of random sources from noisy signals, a problem which is closely related to the Green's function estimation.

1.2. Configuration and procedure. We consider a configuration and an experiment similar to the one described in [13], while motivated by the procedure and study described in [43]; the configuration is illustrated in Figure 1.2. We use $\mathbf{x} \in \mathbb{R}^d$, with $d \in \{1, 2\}$ denoting the lateral spatial dimension, to represent the "lateral" coordinate(s) and $z \in \mathbb{R}_{\geq 0}$ to represent the "principal" or "depth" coordinate; we write $\vec{x} = (z, \mathbf{x})$. The above-mentioned halfspace contains a heterogeneous slab, the random medium, with a large extent in the lateral directions and supported in $(0, z_{\max})$ in the principal direction. The sources are concentrated in the plane $z = 0$ and are independent of the random medium; they model the ambient noise field. The sources are incoherent and statistically stationary. The aperture, or lateral extent, of the source field is denoted A, and its correlation length X_0, while the correlation length of the random medium is denoted l. We observe the signal, u say, that is due to the noisy sources at the points, $\vec{x}_1$ and $\vec{x}_2$, which may be inside or outside ($z > z_{max}$) the random medium, over the time interval $(0, T)$. The key quantity considered is the

cross-correlation function,

$$(1.1) \qquad \mathcal{C}(\tau) = \frac{1}{T} \int_0^T u(t, \vec{x}_1) u(t + \tau, \vec{x}_2) \, dt \, ,$$

for a large time window $(0, T)$. We will also consider the situation with more than two points of observation: $\vec{x}_1, \ldots, \vec{x}_N$, $N \geq 3$.

1.3. Outline. The outline of the paper is as follows. In section 1.2 we discussed the configurational setup that we will consider. In section 2 we describe the modeling of the sources, the medium, and the stochastic paraxial wave equation formulation. Using this model, we analyze the estimation based on (1.1) in section 3. The main result shows that the cross-correlations give the Green's function blurred by a statistically stable "filter"; cf. (3.19). A striking property of the filter is that its support may be much smaller in a random medium than in a (quasi-)homogeneous medium, which is the counterpart of superresolution in this context. In section 4 we develop an approach to localizing a cluster of random sources from noisy signals. The main aspects of the results we derive are general, and we demonstrate this by discussing different scaling regimes in section 5. In subsection 5.4 we touch upon the scaling regime anticipated in applying the analysis to Southeastern Tibet for the estimation of body-wave constituents from ambient noise. We provide some numerical examples in section 6, and concluding remarks in section 7.

2. High-frequency paraxial regime and modeling.

2.1. The random sources. We shall model the ambient or background far field noise in terms of a random field. The impinging noise will be modeled as an initial condition in the plane $z = 0$ supplementing the paraxial evolution equation to be introduced in the next subsection; see Figure 1.2.

Let ν be a random field in $\mathbb{R} \times \mathbb{R}^d$, and χ be a smooth, deterministic, envelope function. We assume that ν has zero mean, is isotropic in $\mathbf{x}$ and stationary, and is independent of the medium with spectrum,

$$(2.1) \qquad \mathbb{E}[\nu(t', \mathbf{x}')\nu(t' + \tau, \mathbf{x}' + \Delta\mathbf{x})] = C_0(\tau, \Delta\mathbf{x}) \, ,$$

and with rapidly decaying correlations. The noisy sources are then collectively modeled as

$$(2.2) \qquad Y(t, \mathbf{x}) = \sigma_y \nu\left(\frac{t}{T_0}, \frac{\mathbf{x}}{X_0}\right) \chi\left(\frac{\mathbf{x} - \mathbf{x}_c}{A}\right) .$$

The envelope function χ models the locality of the sources. We shall consider both an extended source field, with χ having a "large" support, and a concentrated source field, with χ having a "small" support. It is convenient to introduce a characteristic wavelength scale, λ_0, associated with the noise source spectrum,

$$(2.3) \qquad \lambda_0 = c_0 T_0 = \frac{2\pi c_0}{\omega_0} = \frac{2\pi}{k_0} \, ,$$

where T_0 is a characteristic time scale associated with the temporal noise correlations (cf. (2.2)) and c_0 background or homogenized medium wavespeed. Note that the central wavenumber is defined by

$$k_0 = \frac{\omega_0}{c_0} \, .$$

2.2. The parabolic wave equation. In recent decades the parabolic or paraxial wave equation has emerged as the primary tool to describe small scale scattering situations as they appear in radiowave propagation, radar, remote sensing, propagation in urban environments, and in underwater acoustics [29, 32, 41], as well as in propagation problems in the earth's crust [9]. The paraxial equation models wave propagation if the dominant scattering occurs in the direction(s) transverse to a principal propagation direction. Here, we take this model as our starting point and consider propagation in a random medium in the regime of waves propagating over distances that are large compared to the correlation length of the random inhomogeneities and the characteristic wavelength. The relevant wavelength scale is determined by the support of the noise auto-covariance function.

Fundamental to the problem at hand is the role of *scales*. Different scaling relations will give rise to different qualitative behavior of the estimation of the Green's function. The important scales are the following:

- z_1, the characteristic depth (longitudinal distance) from noisy sources to the recordings;
- A, the characteristic size for the support of noisy sources collectively;
- T_0, X_0, the temporal and lateral (spatial) extent of the noise spectrum;
- σ_c, the relative magnitude of medium fluctuations; see (2.5);
- l, the correlation length of the (isotropic) medium fluctuations; see (2.5).

The correlation length corresponds to the dominant spatial scale at which the medium fluctuates, and it typically defines the microscale in the problem.

To introduce the paraxial wave approximation, we consider first the wave equation governing the propagation of acoustic waves:

$$(2.4) \qquad \frac{1}{c^2(\vec{x})} \frac{\partial^2 u}{\partial t^2} - \triangle u = 0, \quad t \in \mathbb{R}, \quad \vec{x} \in \mathbb{R}^{d+1}.$$

Here, the slowness squared, $c^{-2}(z, \mathbf{x})$, is given by

$$(2.5) \qquad c^{-2}(z, \mathbf{x}) = c_0^{-2} \left[1 + \sigma_c \, \mu \left(\frac{z}{l}, \frac{\mathbf{x}}{l} \right) \right],$$

in which μ is a random field modeling the medium fluctuations; c_0 denotes the (deterministic) background wavespeed. In the regime of homogenization, with relatively rapidly fluctuating medium variations, the effective wavespeed is c_0. The regime of homogenization corresponds to the case when the wavelength is large relative to the correlation length of the medium fluctuations, and the propagation distance is on the order of the wavelength. However, in a regime of large propagation distances the effect of the randomness will build up, and this phenomenon will be captured by a random potential, namely through μ, in the paraxial wave equation. We shall here assume that the background wavespeed is constant; see [40] for a discussion of the case with a variable background.

Because "locally" the waves sense a homogeneous medium, it is common practice to introduce the following Fourier transform incorporating the centering in a frame moving with the effective wavespeed,

$$(2.6) \qquad u(t, z, \mathbf{x}) = \frac{1}{2\pi} \int e^{i\omega(z/c_0 - t)} \psi(z, \mathbf{x}, \omega/c_0) \, d\omega,$$

so that the complex amplitude $\psi(z, \mathbf{x}, k)$ satisfies the Helmholtz equation

$$(2.7) \qquad 2ik \frac{\partial \psi}{\partial z} + \triangle_{\mathbf{x}} \psi + k^2(n^2 - 1)\psi = -\frac{\partial^2 \psi}{\partial z^2},$$

with $k = \omega/c_0$ being the wavenumber and $n = n(z, \mathbf{x}) = c_0/c(z, \mathbf{x})$ the random index of refraction relative to the background wavespeed c_0. The fluctuations in the refraction index attain the form

$$(2.8) \qquad n^2(z, \mathbf{x}) - 1 = \sigma_c \, \mu\left(\frac{z}{l}, \frac{\mathbf{x}}{l}\right) .$$

We assume that the fluctuations are modeled by an isotropic and smooth in $\mathbf{x}$, zero mean, stationary rapidly decorrelating random field $\mu(\cdot, \cdot)$, which moreover is Markovian in z. The normalized and dimensionless covariance is given by

$$(2.9) \qquad R(\Delta z, \Delta \mathbf{x}) = \mathbb{E}[\mu(z', \mathbf{x}')\mu(\Delta z + z', \Delta \mathbf{x} + \mathbf{x}')],$$

with $R(0,0) = 1$. We, again, assume rapidly decaying correlations. Note that the dimensionless function R is supported on the $\mathcal{O}(1)$ scale. Thus, the correlation radius of the medium fluctuations is l. We shall consider a specific scaling regime characterized by a certain relation between the parameters that we have introduced in the problem; this scaling regime essentially corresponds to the one introduced in [33]. The regime will follow from the next step where we introduce dimensionless coordinates. To this end, we introduce the characteristic length scales as

- l_x, the characteristic length scale in the lateral direction,
- l_z, the characteristic length scale in the principal (depth) direction.

The following dimensionless parameters will be important in the further analysis:

$$(2.10) \qquad \varepsilon = \frac{l}{l_z}, \quad \delta = \frac{l}{l_x}, \quad \theta = \frac{k_0 l_x^2}{l_z};$$

θ is commonly referred to as the *Rayleigh* number, while ε and δ are the medium correlation length relative to, respectively, characteristic principal and lateral scales. We remark that we specify in (3.5) below how the correlation scale of the ambient noise field relates to these small parameters. The important scaling regime considered here is the *high-frequency paraxial scaling* as introduced in [33], with

$$(2.11) \qquad \frac{1}{\theta} \ll \varepsilon \ll \delta \ll 1.$$

We hasten to add that there are other relevant scaling regimes [2, 5, 18, 34]; we discuss some scaling alternatives in section 5. However, the regime set forth above is characteristic for the estimation problem at hand and captures key aspects of the physical phenomenon under discussion. Note that it follows from our scaling assumptions that $l_x \ll l_z$, which corresponds to the characteristic propagation distance being much larger than the characteristic aperture size and the classical paraxial or beam scaling. This follows, since with $\vec{x}_j = (z_j, \mathbf{x}_j)$ denoting the recording points as before, we shall assume a regime where

$$z'_j = \frac{z_j}{l_z}, \quad \mathbf{x}'_j = \frac{\mathbf{x}_j}{l_x},$$

as well as

$$A' = \frac{A}{l_x}, \quad z'_{\max} = \frac{z_{\max}}{l_z},$$

are fixed, while considering the limits $1/\theta, \varepsilon, \delta \to 0$. The dimensionless coordinates are

$$(2.12) \qquad z' = \frac{z}{l_z}, \quad \mathbf{x}' = \frac{\mathbf{x}}{l_x}, \quad k' = \frac{k}{k_0}, \quad \omega' = \frac{\omega}{\omega_0},$$

and we let

$$(2.13) \qquad t' = \frac{2\pi t}{T_0} = \omega_0 t \,, \quad \overline{c} = \frac{c_0}{\omega_0 l_z} = \frac{1}{k_0 l_z} \,,$$

so that

$$\omega(z/c_0 - t) = \omega'(z'/\overline{c} - t') \,.$$

Note that we have $k' = \omega'$.

In the further analysis, we shall drop the primes in the nondimensionalized coordinates; in dimensionless variables $(z, \mathbf{x}, \omega)$, the paraxial wave equation then becomes

$$(2.14) \qquad 2\mathrm{i}\,(\theta k)\,\frac{\partial \psi}{\partial z} + \triangle_{\mathbf{x}}\psi + \frac{\delta}{\sqrt{\varepsilon}}\,(\theta^2 k^2)\,\mu\!\left(\frac{z}{\varepsilon}, \frac{\mathbf{x}}{\delta}\right)\psi = 0 \,,$$

with $\psi = \psi(z, \mathbf{x}, k)$, upon the identification (cf. (2.7))

$$\sigma_c = \sqrt{\varepsilon}\,\left(\frac{\varepsilon}{\delta}\right) = \sqrt{l/l_z}\,\left(\frac{l_x}{l_z}\right) \,.$$

This is the product of the white noise normalization factor $\sqrt{\varepsilon}$ and the paraxial scaling parameter. These factors are small so that the modeling corresponds to relatively small medium fluctuations. This is exactly the scaling of the fluctuations that gives partly coherent propagation of the wavefield. The fluctuations are sufficiently strong so that the wavefield is affected beyond the homogenization situation, but not so strong that the field completely loses its coherence.

In the scaling regime considered, $\frac{\partial^2 \psi}{\partial z^2}$ on the right-hand side of (2.7) can be neglected. Equation (2.14) is an evolution equation, which is supplemented with the initial conditions (cf. (2.2))

$$(2.15) \qquad \frac{1}{2\pi} \int e^{\mathrm{i}\omega(-t)}\psi(z = 0, \mathbf{x}, \omega)\,d\omega = Y\,(T_0 t, l_x \mathbf{x}) \,.$$

Indeed, the paraxial field ψ satisfies an initial value problem rather than a boundary value problem as in the case of the Helmholtz equation. This reflects the fact that we consider a regime where lateral scattering is dominant over scattering along the principal direction.

2.3. White noise model. We shall consider functionals of the field, ψ, in the scaling regime in (2.11). Following [33], we introduce the Wigner distribution:

$$(2.16) \qquad W_\theta(z, \mathbf{x}, \mathbf{p}; \omega) = \iint \frac{1}{(2\pi)^d} e^{\mathrm{i}\mathbf{p}\cdot\mathbf{y}} \psi\!\left(z, \mathbf{x} - \frac{\mathbf{y}}{2\theta}, \omega\right) \psi\!\left(z, \mathbf{x} + \frac{\mathbf{y}}{2\theta}, \omega\right)^{*} d\mathbf{y} \,,$$

where we have used "*" to represent complex conjugation. It can then be shown [17, 33] that in the *high-frequency* $(\theta \to \infty)$ and *white noise* $(\varepsilon \to 0)$ limit, the limiting Wigner transform that we denote as W_δ is characterized weakly (in law) by the Itô–Liouville stochastic partial differential equation, as follows.

PROPOSITION 2.1. *The Wigner distribution W_θ converges in the limit $1/\theta \to 0$ followed by $\varepsilon \to 0$ weakly in law to the process W_δ solving*

$$(2.17) \qquad dW_\delta = \left[-\frac{\mathbf{p}}{k}\cdot\nabla_{\mathbf{x}}W_\delta + \frac{k^2 D}{2}\triangle_{\mathbf{p}}W_\delta\right] dz - \frac{k}{2}\nabla_{\mathbf{p}}W_\delta \cdot d\mathbf{B}\left(z, \frac{\mathbf{x}}{\delta}\right) .$$

Here, $\mathbf{B}(\mathbf{x}, z)$ is a vector-valued Brownian field with covariance

$$(2.18) \qquad \mathbb{E}[B_i(z_1, \mathbf{x}_1)B_j(z_2, \mathbf{x}_2)] = -\left(\frac{\partial^2 R_0(\mathbf{x}_1 - \mathbf{x}_2)}{\partial x_i \partial x_j}\right) z_1 \wedge z_2\,,$$

where $z_1 \wedge z_2 = \min\{z_1, z_2\}$; in the assumed isotropic case, we have (cf. (2.9))

$$(2.19) \qquad D = -\frac{R_0''(0)}{4}, \quad \text{with } R_0(\mathbf{x}) = \int_{-\infty}^{\infty} R(\zeta, \mathbf{x})\, d\zeta\,.$$

We remark that the second derivative of the (isotropic) medium correlation function is negative: $R_0''(0) < 0$ so that indeed (2.17) is well posed. It now follows directly from (2.17) that the mean, $\overline{W} = \mathbb{E}[W_\delta]$, is independent of δ and solves the advection-diffusion equation

$$(2.20) \qquad \frac{\partial \overline{W}}{\partial z} + \frac{\mathbf{p}}{k} \cdot \nabla_{\mathbf{x}} \overline{W} = \frac{k^2 D}{2} \triangle_{\mathbf{p}} \overline{W}\,.$$

The explicit expression for the Green's function of (2.20) is

$$U(z, \mathbf{x}, \mathbf{p}; \mathbf{x}_0, \mathbf{p}_0) = \iint \frac{1}{\omega^d (2\pi)^{2d}} \exp\left(i\left[\mathbf{w} \cdot (\mathbf{x} - \mathbf{x}_0) + \mathbf{r} \cdot \frac{(\mathbf{p} - \mathbf{p}_0)}{\omega} - z\mathbf{w} \cdot \frac{\mathbf{p}_0}{\omega}\right]\right)$$

$$(2.21) \qquad\qquad \times \exp\left(-\frac{Dz}{2}\left[r^2 + z\mathbf{r} \cdot \mathbf{w} + \frac{w^2 z^2}{3}\right]\right) d\mathbf{w}\, d\mathbf{r}\,,$$

with $r = \|\mathbf{r}\|_2$ and $w = \|\mathbf{w}\|_2$. This expression will be useful in order to characterize how the computed cross-correlations relate to the propagation Green's function of interest. That the computed cross-correlations give a stable and "low noise" estimate of the Green's function shall emerge as a consequence of assuming a stabilization regime. Indeed, here we shall assume the *stabilization* regime corresponding to the limit $\delta \to 0$, as discussed in [33]. The robust estimation of the empirical Green's function will be a consequence of the following stabilization result.

PROPOSITION 2.2. *Assume that the initial Wigner distribution, $W_I(\mathbf{x}, \mathbf{p})$, is uniformly bounded and Lipschitz continuous. Define*

$$(2.22) \qquad I_\delta(z, \mathbf{x}, \mathbf{y}) = \iint W_\delta(z, \mathbf{x}, \mathbf{p}) e^{-i\mathbf{p} \cdot \mathbf{y}}\, d\mathbf{p}.$$

Then

$$(2.23) \qquad \lim_{\delta \to 0} \mathbb{E}\left\{I_\delta^2(z, \mathbf{x}, \mathbf{y})\right\} = \mathbb{E}^2\left\{I_\delta(z, \mathbf{x}, \mathbf{y})\right\},$$

where $\mathbb{E}\left\{I_\delta(z, \mathbf{x}, \mathbf{y})\right\}$ is independent of δ.

This result is a slight generalization of the stability result derived in [33]; see the appendix.

3. Analysis of cross-correlations.

3.1. Time averaging. The quantity of interest is the cross-correlation function,

$$(3.1) \qquad \mathcal{C}_{\mathcal{H}}(\tau, \vec{x}_1, \vec{x}_2) = \int \mathcal{H}(t)\, u(t, \vec{x}_1) u(t + \tau, \vec{x}_2)\, dt\,,$$

in which $\mathcal{H}$ is a time-window function; cf. (1.1). Here, u is modeled from the solution of the paraxial wave equation (cf. (2.14)) subject to initial conditions (2.15). We introduce the notation $\check{v}$ for the partial Fourier transform of v with respect to time, and $\widehat{v}$ for the complete transform:

$$v(t, \mathbf{x}) = \frac{1}{2\pi} \int e^{-\mathrm{i}\omega t} \check{v}(\omega, \mathbf{x})\, d\omega = \frac{1}{(2\pi)^{d+1}} \iint e^{-\mathrm{i}(\omega t - \mathbf{p} \cdot \mathbf{x})} \widehat{v}(\omega, \mathbf{p})\, d\mathbf{p}\, d\omega\,.$$

Let G_θ be the Green's function associated with the paraxial wave equation (2.14); then we have in the standardized variables

$$(3.2) \qquad u(t, \vec{x}) = \iint \widetilde{G}_\theta(t - s, \vec{x}; \vec{x}_n)\, Y(T_0 s, l_x \mathbf{x}_n)\, d\mathbf{x}_n ds,$$

where $\vec{x}_n = (0, \mathbf{x}_n)$ and

$$(3.3) \qquad \widetilde{G}_\theta(t, z, \mathbf{x}; 0, \mathbf{x}_n) = \frac{1}{2\pi} \int e^{\mathrm{i}\omega(z/\overline{c} - t)} G_\theta(\omega, z, \mathbf{x}; 0, \mathbf{x}_n)\, d\omega$$

(cf. (2.6)). Substituting (3.2) into (3.1) yields

$$(3.4) \quad \mathcal{C}_\mathcal{H}(\tau, \vec{x}_1, \vec{x}_2) = \iint \mathcal{H}(t) \widetilde{G}_\theta(t - s_1, \vec{x}_1; \vec{x}_{n_1}) Y(T_0 s_1, l_x \mathbf{x}_{n_1})$$
$$\times\, \widetilde{G}_\theta(t + \tau - s_2, \vec{x}_2; \vec{x}_{n_2}) Y(T_0 s_2, l_x \mathbf{x}_{n_2})\, dt\, ds_1\, ds_2\, d\mathbf{x}_{n_1}\, d\mathbf{x}_{n_2}\,.$$

Note that by the result (2.20) the paraxial field decorrelates laterally on the scale $1/\theta$. We now assume that the ambient noise field decorrelates on this scale by choosing

$$(3.5) \qquad X_0 = \frac{l_x}{\theta}\,.$$

When we substitute (2.2) into (3.4), we then obtain

$$(3.6) \quad \mathcal{C}_\mathcal{H}(\tau, \vec{x}_1, \vec{x}_2) = \iint \sigma_y^2 \left\{ \int \mathcal{H}(t)\nu(t - v_1, \theta\mathbf{x}_{n_1})\, \nu(t - v_2, \theta\mathbf{x}_{n_2})\, dt \right\}$$
$$\times\, \widetilde{G}_\theta(v_1, \vec{x}_1; \vec{x}_{n_1}) \widetilde{G}_\theta(v_2 + \tau, \vec{x}_2; \vec{x}_{n_2}) \chi\left(\frac{\mathbf{x}_{n_1} - \mathbf{x}_c}{A} \right) \chi\left(\frac{\mathbf{x}_{n_2} - \mathbf{x}_c}{A} \right)\, dv_1\, dv_2\, d\mathbf{x}_{n_1}\, d\mathbf{x}_{n_2}\,.$$

We may choose for $\mathcal{H}$ the indicator function

$$\mathcal{H}_T(\cdot) = \frac{\mathcal{I}_{\left(-\frac{T}{2}, \frac{T}{2}\right)}(\cdot)}{T}\,;$$

then

$$\lim_{T \to \infty} \int_{-\infty}^{\infty} \mathcal{H}_T(t)\nu(t - v_1, \theta\mathbf{x}_{n_1})\, \nu(t - v_2, \theta\mathbf{x}_{n_2})\, dt = C_0(v_2 - v_1, \theta(\mathbf{x}_{n_2} - \mathbf{x}_{n_1}))\,,$$

the mean square with respect to the distribution of the impinging noise sources. Our interest is in such a regime where the time average effectively removes the fluctuations in the quantity of interest, *exploiting the randomness of the sources.* Substituting the above average into (3.6) leads to the introduction of

$$(3.7) \quad \langle \mathcal{C} \rangle_\theta (\tau, \vec{x}_1, \vec{x}_2) = \iint \sigma_y^2 C_0(v_2 - v_1, \theta(\mathbf{x}_{n_2} - \mathbf{x}_{n_1}))$$
$$\times\, \widetilde{G}_\theta(v_1, \vec{x}_1; \vec{x}_{n_1}) \widetilde{G}_\theta(v_2 + \tau, \vec{x}_2; \vec{x}_{n_2}) \chi\left(\frac{\mathbf{x}_{n_1} - \mathbf{x}_c}{A} \right) \chi\left(\frac{\mathbf{x}_{n_2} - \mathbf{x}_c}{A} \right)\, dv_1\, dv_2\, d\mathbf{x}_{n_1}\, d\mathbf{x}_{n_2}\,.$$

3.2. Green's function filter and limits. We obtain the following representation for the quantity of interest.

PROPOSITION 3.1. *Let* $\langle \mathcal{C} \rangle_\theta$ *be as in* (3.7), *and assume the relative ordering*

$$z_1 < z_2 \, .$$

Then

(3.8)
$$\langle \mathcal{C} \rangle_\theta (\tau, \vec{x}_1, \vec{x}_2) \;=\; \iint \widetilde{G}_\theta \left(\tau - s, z_2, \mathbf{x}_2; z_1, \mathbf{x}_1 - \frac{\mathbf{y}}{\theta} \right) \Lambda_\theta \left(z_1, s, \mathbf{x}_1 - \frac{\mathbf{y}}{2\theta}, \mathbf{y} \right) ds \, d\mathbf{y},$$

in which

$$
\Lambda_\theta(z, \tau, \mathbf{x}, \mathbf{y}) = \int \frac{e^{-\mathrm{i}\omega\tau}}{2\pi} \left\{ \iint \sigma_y^2 \check{C}_0(\omega, \theta(\mathbf{x}_{n_2} - \mathbf{x}_{n_1})) \right.
$$
(3.9)
$$
\times \, G_\theta \left(\omega, z, \mathbf{x} - \frac{\mathbf{y}}{2\theta}; 0, \mathbf{x}_{n_2} \right) G_\theta \left(\omega, z, \mathbf{x} + \frac{\mathbf{y}}{2\theta}; 0, \mathbf{x}_{n_1} \right)^*
$$
$$
\left. \times \, \chi \left(\frac{\mathbf{x}_{n_1} - \mathbf{x}_c}{A} \right) \chi \left(\frac{\mathbf{x}_{n_2} - \mathbf{x}_c}{A} \right) d\mathbf{x}_{n_1} \, d\mathbf{x}_{n_2} \right\} \theta^{-d} \, d\omega \, .
$$

Here, Λ_θ *is referred to as the Green's function filter.*

Proof. We begin with substituting (3.3) into (3.7), and we obtain

(3.10) $\langle \mathcal{C} \rangle_\theta (\tau, \vec{x}_1, \vec{x}_2) = (2\pi)^{-2} \iint \sigma_y^2 C_0(v_2 - v_1, \theta(\mathbf{x}_{n_2} - \mathbf{x}_{n_1}))$

$$
\times \, G_\theta(\omega_1, z_1, \mathbf{x}_1; 0, \mathbf{x}_{n_1})^* e^{\mathrm{i}\omega_1(v_1 - z_1/\overline{c})} \, G_\theta(\omega_2, z_2, \mathbf{x}_2; 0, \mathbf{x}_{n_2}) e^{-\mathrm{i}\omega_2((v_2 + \tau) - z_2/\overline{c})}
$$
$$
\times \, \chi \left(\frac{\mathbf{x}_{n_1} - \mathbf{x}_c}{A} \right) \chi \left(\frac{\mathbf{x}_{n_2} - \mathbf{x}_c}{A} \right) dv_1 \, dv_2 \, d\mathbf{x}_{n_1} \, d\mathbf{x}_{n_2} \, d\omega_1 \, d\omega_2 \, ,
$$

where we made use of the fact that $\widetilde{G}_\theta$ is real-valued. We carry out the integration over v_1 yielding a Fourier transform of C_0 with respect to its time argument; the integration over v_2 then gives a factor $\delta(\omega_2 - \omega_1)$:

(3.11) $\langle \mathcal{C} \rangle_\theta (\tau, \vec{x}_1, \vec{x}_2) = (2\pi)^{-2} \iint \sigma_y^2 \check{C}_0(\omega_1, \theta(\mathbf{x}_{n_2} - \mathbf{x}_{n_1}))$

$$
\times \, G_\theta(\omega_1, z_1, \mathbf{x}_1; 0, \mathbf{x}_{n_1})^* G_\theta(\omega_2, z_2, \mathbf{x}_2; 0, \mathbf{x}_{n_2}) \, e^{-\mathrm{i}((\omega_2 - \omega_1)v_2 + \omega_2\tau)} e^{\mathrm{i}(\omega_2 z_2 - \omega_1 z_1)/\overline{c}}
$$
$$
\times \, \chi \left(\frac{\mathbf{x}_{n_1} - \mathbf{x}_c}{A} \right) \chi \left(\frac{\mathbf{x}_{n_2} - \mathbf{x}_c}{A} \right) dv_2 \, d\mathbf{x}_{n_1} \, d\mathbf{x}_{n_2} \, d\omega_1 \, d\omega_2
$$
$$
= (2\pi)^{-1} \iint \sigma_y^2 \check{C}_0 \left(\omega, \theta(\mathbf{x}_{n_2} - \mathbf{x}_{n_1}) \right) e^{-\mathrm{i}\omega(\tau - (z_2 - z_1)/\overline{c})}
$$
$$
\times \, G_\theta(\omega, z_1, \mathbf{x}_1; 0, \mathbf{x}_{n_1})^* G_\theta(\omega, z_2, \mathbf{x}_2; 0, \mathbf{x}_{n_2})
$$
$$
\times \, \chi \left(\frac{\mathbf{x}_{n_1} - \mathbf{x}_c}{A} \right) \chi \left(\frac{\mathbf{x}_{n_2} - \mathbf{x}_c}{A} \right) d\mathbf{x}_{n_1} \, d\mathbf{x}_{n_2} \, d\omega \, .
$$

We invoke the semigroup property of the solution operator to the paraxial wave equation, and, using that $z_2 > z_1$, we get

$$(3.12) \quad \langle \mathcal{C} \rangle_\theta (\tau, \vec{x}_1, \vec{x}_2) = \iint \frac{e^{-i\omega(\tau-(z_2-z_1)/\overline{c})}}{2\pi} \left\{ \iint \sigma_y^2 \check{C}_0(\omega, \theta(\mathbf{x}_{n_2} - \mathbf{x}_{n_1})) \right.$$

$$\times G_\theta(\omega, z_1, \mathbf{x}_1; 0, \mathbf{x}_{n_1})^* G_\theta(\omega, z_1, \mathbf{y}; 0, \mathbf{x}_{n_2}) \chi\left(\frac{\mathbf{x}_{n_1} - \mathbf{x}_c}{A}\right) \chi\left(\frac{\mathbf{x}_{n_2} - \mathbf{x}_c}{A}\right) d\mathbf{x}_{n_1} d\mathbf{x}_{n_2} \left. \right\}$$

$$\times G_\theta(\omega, z_2, \mathbf{x}_2; z_1, \mathbf{y}) \, d\omega \, d\mathbf{y} \, .$$

We then change variables of integration,

$$(3.13) \quad \langle \mathcal{C} \rangle_\theta (\tau, \vec{x}_1, \vec{x}_2) = \iint \frac{e^{-i\omega(\tau-(z_2-z_1)/\overline{c})}}{2\pi} \left\{ \iint \sigma_y^2 \check{C}_0(\omega, \theta(\mathbf{x}_{n_2} - \mathbf{x}_{n_1})) \right.$$

$$\times G_\theta(\omega, z_1, \mathbf{x}_1; 0, \mathbf{x}_{n_1})^* G_\theta\left(\omega, z_1, \mathbf{x}_1 - \frac{\mathbf{y}}{\theta}; 0, \mathbf{x}_{n_2}\right)$$

$$\times \chi\left(\frac{\mathbf{x}_{n_1} - \mathbf{x}_c}{A}\right) \chi\left(\frac{\mathbf{x}_{n_2} - \mathbf{x}_c}{A}\right) d\mathbf{x}_{n_1} d\mathbf{x}_{n_2} \left. \right\} G_\theta\left(\omega, z_2, \mathbf{x}_2; z_1, \mathbf{x}_1 - \frac{\mathbf{y}}{\theta}\right) \theta^{-d} \, d\omega \, d\mathbf{y}$$

$$= \iint \frac{e^{-i\omega(\tau-(z_2-z_1)/\overline{c})}}{2\pi} G_\theta\left(\omega, z_2, \mathbf{x}_2; z_1, \mathbf{x}_1 - \frac{\mathbf{y}}{\theta}\right) \check{\Lambda}_\theta\left(z_1, \omega, \mathbf{x}_1 - \frac{\mathbf{y}}{2\theta}, \mathbf{y}\right) d\omega \, d\mathbf{y} \, ,$$

which gives the result (3.8).   ☐

We will now make the following assumption.

ASSUMPTION 1.

$$(3.14) \qquad\qquad\qquad \sigma_y^2 = \theta^d \, .$$

The expression (3.9) then simplifies, and this assumption corresponds to letting the correlation radius of the impinging noise field be θ independent.

We remark that the paraxial Green's function will decorrelate in the lateral dimensions on the $1/\theta$ scale, and that this is the motivation for the choice of parameterization of the filter Λ_θ.

It will prove natural to introduce the Wigner distribution

$$(3.15) \quad W_\theta(z, \mathbf{x}, \mathbf{p}; \omega) = \iint \frac{e^{i\mathbf{p}\cdot\mathbf{y}}}{(2\pi)^d} G_\theta\left(\omega, z, \mathbf{x} - \frac{\mathbf{y}}{2\theta}; 0, \mathbf{x}_{n_2}\right) G_\theta\left(\omega, z, \mathbf{x} + \frac{\mathbf{y}}{2\theta}; 0, \mathbf{x}_{n_1}\right)^*$$

$$\times \check{C}_0(\omega, \theta(\mathbf{x}_{n_2} - \mathbf{x}_{n_1})) \chi\left(\frac{\mathbf{x}_{n_1} - \mathbf{x}_c}{A}\right) \chi\left(\frac{\mathbf{x}_{n_2} - \mathbf{x}_c}{A}\right) d\mathbf{x}_{n_1} d\mathbf{x}_{n_2} \, d\mathbf{y} \, ,$$

so that

$$(3.16) \qquad\qquad \check{\Lambda}_\theta(z, \omega, \mathbf{x}, \mathbf{y}) = \iint W_\theta(z, \mathbf{x}, \mathbf{p}; \omega) e^{-i\mathbf{p}\cdot\mathbf{y}} d\mathbf{p} \, .$$

This Wigner distribution coincides with the one given in (2.16) subject to initial conditions that derive from (2.15), which follows from (2.6), (3.2), and (3.3). In the high-frequency ($\theta \to \infty$) and white noise ($\varepsilon \to 0$) limits, the Wigner distribution in (3.15) is characterized weakly (in law) by (2.17), while its mean satisfies (2.20).

The initial condition, at $z = 0$, for the Wigner distribution follows directly from the corresponding initial condition for the Green's function G_θ:

$$(3.17) \quad W_\theta(0, \mathbf{x}, \mathbf{p}; \omega) = \iint \frac{e^{i\theta \mathbf{p} \cdot 2(\mathbf{x} - \mathbf{x}_{n_2})}}{(2\pi)^d} \check{C}_0(\omega, \theta(2(\mathbf{x}_{n_2} - \mathbf{x})))$$

$$\times \, \chi\left(\frac{2\mathbf{x} - \mathbf{x}_{n_2} - \mathbf{x}_c}{A}\right) \chi\left(\frac{\mathbf{x}_{n_2} - \mathbf{x}_c}{A}\right) \theta^d \, d\mathbf{x}_{n_2}$$

$$\sim \widehat{C}_0(\omega, \mathbf{p}) \frac{\chi^2\left(\frac{\mathbf{x} - \mathbf{x}_c}{A}\right)}{(4\pi)^d} \equiv W_I(\mathbf{x}, \mathbf{p}; \omega) \quad \text{as } \theta \to \infty.$$

We will apply this approximation below.

We now use the Green's function (2.21), and initial condition (3.17), in (3.16) and define the following Green's function filter,

$$\check{\Lambda}(z, \omega, \mathbf{x}, \mathbf{y}) = \iint \frac{e^{-i\mathbf{p} \cdot \mathbf{y}}}{(2\pi)^{2d}} \exp\left(i\left[\mathbf{w} \cdot (\mathbf{x} - \mathbf{x}_0) + \mathbf{r} \cdot \frac{(\mathbf{p} - \mathbf{p}_0)}{\omega} - z\mathbf{w} \cdot \frac{\mathbf{p}_0}{\omega}\right]\right)$$

$$\times \exp\left(-\frac{Dz}{2}\left[r^2 + z\mathbf{r} \cdot \mathbf{w} + \frac{w^2 z^2}{3}\right]\right) \widehat{C}_0(\omega, \mathbf{p}_0)$$

$$\times \frac{\chi^2\left(\frac{\mathbf{x}_0 - \mathbf{x}_c}{A}\right)}{(4\pi)^d} \omega^{-d} \, d\mathbf{w} \, d\mathbf{r} \, d\mathbf{p} \, d\mathbf{x}_0 \, d\mathbf{p}_0$$

$$= \frac{1}{(4\pi)^d} \iint e^{i\omega \mathbf{w} \cdot (\mathbf{x} - \mathbf{x}_c)} \exp\left(-\frac{\omega^2 Dz}{2}\left[y^2 + z\mathbf{y} \cdot \mathbf{w} + \frac{w^2 z^2}{3}\right]\right)$$

$$(3.18) \qquad \times \, \check{C}_0(\omega, \mathbf{y} + z\mathbf{w}) \widehat{\chi}_A(\omega \mathbf{w}) \, \omega^d \, d\mathbf{w},$$

in which

$$\widehat{\chi}_A(\mathbf{w}) = \iint e^{-i\mathbf{w} \cdot \mathbf{x}_0} \chi^2\left(\frac{\mathbf{x}_0}{A}\right) d\mathbf{x}_0.$$

The characterization of a statistically stable filter now follows from the representation (3.16) and Propositions 2.1 and 2.2, as follows.

PROPOSITION 3.2. *The deterministic Green's function filter converges to a deterministic filter*

$$(3.19) \qquad\qquad \lim_{\delta \to 0} \lim_{\varepsilon \to 0} \lim_{\theta \to \infty} \check{\Lambda}_\theta(z, \omega, \mathbf{x}, \mathbf{y}) = \check{\Lambda}(z, \omega, \mathbf{x}, \mathbf{y})$$

in $L^2(\mathbb{P})$.

3.3. Effective filter. In order to obtain qualitative and quantitative insight on the Green's function filtering behavior, we shall assume that the spectrum of the envelope function and the spectrum of the noise covariance have Gaussian shapes. That is, we shall assume

$$(3.20) \qquad\qquad \chi(\mathbf{x}) = \frac{1}{(2\pi)^{d/2}} e^{-\frac{|\mathbf{x}|^2}{2}}, \quad \check{C}_0(\omega, \mathbf{y}) = \widehat{f}_0(\omega) e^{\frac{-|\mathbf{y}|^2}{2\sigma_x^2}}.$$

We recall that the filter will be evaluated at $z = z_1$, corresponding to the longitudinal distance from the source plane to the first recording point. We find that then

$$\check{\Lambda}(z, \omega, \mathbf{x}, \mathbf{y}) = \left(\frac{A}{4\pi\sqrt{2}}\right)^d \omega^d \widehat{f}_0(\omega) \iint e^{i\omega \mathbf{w} \cdot (\mathbf{x} - \mathbf{x}_c)} \exp\left(-\frac{\omega^2 Dz}{2}\left[y^2 + z\mathbf{y} \cdot \mathbf{w} + \frac{w^2 z^2}{3}\right]\right)$$

$$\times \, e^{\frac{-|\mathbf{y} + z\mathbf{w}|^2}{2\sigma_x^2}} e^{\frac{-\omega^2 |\mathbf{w}|^2 A^2}{4}} \, d\mathbf{w}.$$

We rewrite this expression as

(3.21)

$$\check{\Lambda}(z,\omega,\mathbf{x},\mathbf{y}) = \left(\frac{A}{4\pi\sqrt{2}}\right)^d \omega^d \widehat{f_0}(\omega) \iint e^{i\omega\mathbf{w}\cdot(\mathbf{x}-\mathbf{x}_c)} e^{-\omega^2\left(a_1 w^2 + 2a_2\mathbf{y}\cdot\mathbf{w} + a_3 y^2\right)/2}\,d\mathbf{w}$$

$$= \left(\frac{A^2}{16\pi a_1}\right)^{d/2} \widehat{f_0}(\omega) e^{-\frac{|\mathbf{x}-\mathbf{x}_c|^2}{2a_1}} e^{-\omega^2(a_3 - a_2^2/a_1)y^2/2} e^{-i\omega(a_2/a_1)\mathbf{y}\cdot(\mathbf{x}-\mathbf{x}_c)}$$

with

$$a_1(\omega) = \frac{A^2}{2} + \frac{z^2}{\omega^2\sigma_x^2} + \frac{Dz^3}{3}, \quad a_2(\omega) = \frac{z}{\omega^2\sigma_x^2} + \frac{Dz^2}{2}, \quad a_3(\omega) = \frac{1}{\omega^2\sigma_x^2} + Dz\,.$$

Furthermore, we shall assume that the noise source field has a temporal frequency spectrum of the form

(3.22) $$\widehat{f_0}(\omega) = \frac{1}{2}\left(\widehat{f}\left(T_s(\omega - \omega_c)\right) + \widehat{f}\left(T_s(\omega + \omega_c)\right)\right).$$

We can now associate two characteristic length scales and one characteristic temporal scale with the Green's function filter in the narrow band situation so that T_s is large:

- The *refocusing* length scale

$$l_f(\omega_c) = \frac{\lambda_c}{2\pi\sqrt{a_3(\omega_c) - \frac{a_2^2(\omega_c)}{a_1(\omega_c)}}}$$

$$= \frac{\lambda_c}{2\pi}\left(\frac{\frac{A^2}{2} + \frac{\lambda_c^2 z^2}{4\pi^2\sigma_x^2} + \frac{Dz^3}{3}}{\left(A^2 + \frac{Dz^3}{6}\right)\frac{Dz}{2} + \left(\frac{A^2}{2} + \frac{Dz^3}{3}\right)\frac{\lambda_c^2}{4\pi^2\sigma_x^2}}\right)^{1/2},$$

  for

$$\lambda_c = 2\pi/\omega_c$$

  with ω_c a characteristic frequency of the noise source spectrum. This length scale determines the smoothing scale in the spatial source coordinates of the Green's function estimate, since the Green's function is blurred on the scale l_f/θ; see (3.19), (3.21). Note that in the low-frequency limit with $\lambda_c \to \infty$ the estimate of the Green's function degrades since the refocusing length scale becomes large in this limit.

- The *effective aperture* length scale

$$l_a(\omega_c) = \sqrt{a_1(\omega_c)} = \sqrt{\frac{A^2}{2} + \frac{\lambda_c^2 z^2}{4\pi^2\sigma_x^2} + \frac{Dz^3}{3}}\,.$$

  This corresponds to the lateral range, relative to the center $\mathbf{x}_c$, of impinging noise sources contributing to the Green's function estimate through $\langle\mathcal{C}\rangle_\theta$. If the lateral separation between $\mathbf{x}_j$ and $\mathbf{x}_c$ is large relative to this length, then the filter will weaken the Green's function significantly. In the limit $\lambda_c \to 0$, l_a corresponds to the effective aperture in [33].

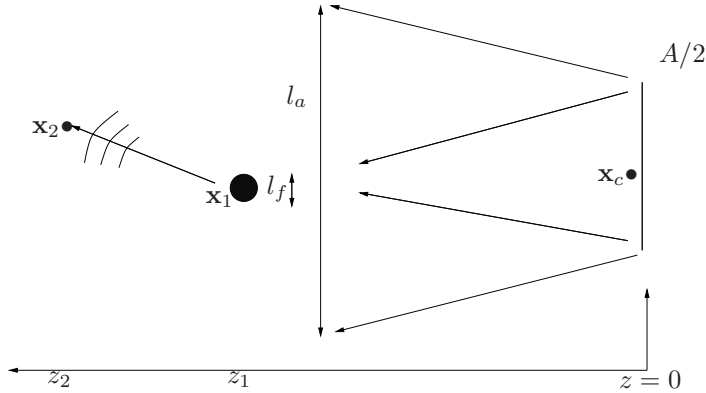FIG. 3.1. *The effective aperture l_a and the refocusing length scale l_f.*

- The Green's function will be blurred in time, on the scale T_s, corresponding to the support of the ambient noise correlations in time.

The characteristic length scales are illustrated in Figure 3.1.

We comment on how the characteristic length scales depend on some of the parameters. In the case of a homogeneous medium, with $D = 0$ and low frequencies, we have

$$l_f(\omega_c)|_{D=0} \overset{\lambda_c \to \infty}{\sim} \left(\frac{\lambda_c z}{A}\right) \frac{1}{\sqrt{2\pi}},$$

which corresponds to the classical *Rayleigh* resolution. While in the high-frequency limit and homogeneous medium case, with $D = 0$, we find

$$l_f(\omega_c)|_{D=0} \overset{\lambda_c \to 0}{\sim} \sigma_x,$$

that is, a length scale corresponding to that of the support of the ambient noise field in the lateral spatial dimensions. Next, we consider the limit of (relatively) strong medium fluctuations:

$$l_f(\omega_c) \overset{D \to \infty}{\sim} \frac{\lambda_c}{\pi\sqrt{zD}},$$

which leads to a small refocusing scale.

4. Source location estimation. Here, we consider the case of narrow noise aperture, A, and discuss the problem of estimating the "source location" $\mathbf{x}_c$. We assume that the points of observation lie in the plane $z_2 = z_1 = z$. From (3.8) we then find that

$$\langle \mathcal{C} \rangle_\theta (\tau, z, \mathbf{x}_1, z, \mathbf{x}_2) = \theta^d \int \frac{e^{-i\omega\tau}}{2\pi} \check{\Lambda}_\theta(z, \omega, \tfrac{1}{2}(\mathbf{x}_1 + \mathbf{x}_2), \theta(\mathbf{x}_1 - \mathbf{x}_2)) \, d\omega.$$

For two points separated on the $1/\theta$ scale, we write

(4.1)
$$\mathbf{x}_1 = \mathbf{x} + \frac{\mathbf{y}}{2\theta}, \quad \mathbf{x}_2 = \mathbf{x} - \frac{\mathbf{y}}{2\theta}.$$

In the case of source estimation, we replace assumption (3.14) by the following.

ASSUMPTION 2.
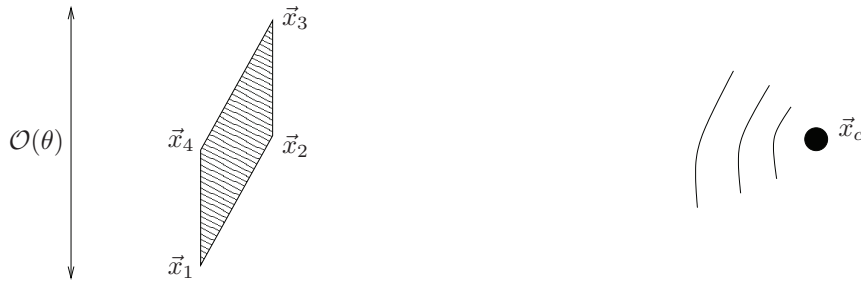
(4.2)
$$\sigma_y^2 \equiv 1.$$

FIG. 4.1. *Estimation of source location: By computing the cross-correlations between the points* $\vec{x}_1, \ldots, \vec{x}_4$ *on the mirror, one obtains differential traveltimes, corresponding to* $|\vec{x}_i - \vec{x}_c| - |\vec{x}_j - \vec{x}_c|$, *which can be used to estimate the source location* $\vec{x}_c$.

Thus, the magnitude of the localized noise source field is now θ independent. We then have

$$\langle \mathcal{C} \rangle_\theta \left(\tau, z, \mathbf{x} + \frac{\mathbf{y}}{2\theta}, z, \mathbf{x} - \frac{\mathbf{y}}{2\theta} \right) = \int \frac{e^{-i\omega\tau}}{2\pi} \iint W_\theta(z, \mathbf{x}, \mathbf{p}; \omega) e^{-i\mathbf{p}\cdot\mathbf{y}} d\mathbf{p},$$

and it follows by Proposition 2.2 that $\langle \mathcal{C} \rangle_\theta$ is statistically stable.

We consider, moreover, a tight lateral support for the noise field correlations: $\sigma_x \ll 1$ in the model (3.20). Then, using Proposition 3.2 and (3.18), we obtain

$$\sigma_x^{-d} \langle \mathcal{C} \rangle_\theta \left(\tau, z, \mathbf{x} + \frac{\mathbf{y}}{\theta}, z, \mathbf{x} - \frac{\mathbf{y}}{\theta} \right)$$

$$\sim \left(\frac{A^2}{16\pi z^2} \right)^{d/2} \int |\omega|^d \widehat{f}_0(\omega) \frac{e^{-i\omega\tau}}{2\pi} e^{-\frac{\omega^2 \sigma_a^2 y^2}{2}} e^{-i\omega \mathbf{y}\cdot(\mathbf{x}-\mathbf{x}_c)/z} \, d\omega$$

$$= \left\{ \left(\frac{A^2}{16\pi z^2} \right)^{d/2} \widetilde{f}(\cdot) * \mathcal{N}_{\sigma_a}(\cdot) \right\} \left(\tau + \mathbf{y} \cdot \frac{\mathbf{x} - \mathbf{x}_c}{z} \right),$$

where "$*$" denotes convolution, $\mathcal{N}_\sigma$ is the Gaussian distribution with standard deviation σ, and we define

$$\sigma_a = \sqrt{\frac{A^2}{2z^2} + \frac{Dz}{3}},$$

$$\widetilde{f}(\tau) = \int \frac{e^{-i\omega\tau}}{2\pi} |\omega|^d \widehat{f}_0(\omega) \, d\omega.$$

We remark that in the paraxial regime we have

$$(4.3) \qquad \tau + \mathbf{y}\cdot(\mathbf{x}-\mathbf{x}_c)/z = \frac{2\pi}{T_0} \left\{ \widetilde{t} + \left(\frac{|\widetilde{\mathbf{x}}_1 - \widetilde{\mathbf{x}}_c|^2}{2\widetilde{z}c_0} - \frac{|\widetilde{\mathbf{x}}_2 - \widetilde{\mathbf{x}}_c|^2}{2\widetilde{z}c_0} \right) \right\} \approx \frac{2\pi}{T_0} \left(\widetilde{t} + (\widetilde{\tau}_{s1} - \widetilde{\tau}_{s2}) \right),$$

with $\widetilde{t}, \widetilde{z}, \widetilde{\mathbf{x}}_j$, and $\widetilde{\mathbf{x}}_j$ denoting the original scaled coordinates and $\widetilde{\tau}_{sj}$ being the traveltime from the noise source at $\vec{x}_c$ to observation point $\vec{x}_j$. Thus, given observations at array points $\vec{x}_1, \ldots, \vec{x}_4$, separated as in (4.1), one can estimate the location of the source via differential traveltime estimates in the $(d+1) = 3$-dimensional case; see Figure 4.1. The resolution of the estimate is limited by the support of the noise correlation function, the strength of the medium fluctuations, and the aperture A. We remark that in contrast to the situation where one aims at estimating the Green's function, here, a large value for σ_a leads to a poor resolution.

5. White noise paraxial regimes and applications. In this section, we discuss alternative scaling scenarios that have been introduced in [34] and [20]. We demonstrate the robustness of the results derived above by showing that their essential features prevail under a wide range of scaling scenarios. Indeed, the general analysis will be the same, but the Green's function filter changes through replacing the function U in (2.21) by the Green's function associated with the relevant modification of (2.20). In subsection 5.4 we conclude the discussion on scaling scenarios by considering a particular application, namely, body-wave scattering in Southeastern Tibet motivated in the introduction, and its characteristic scales.

We consider a scaling and a nondimensionalization as above. We shall here discuss the situation with $\varepsilon \to 0$ being the smallest parameter. This limit gives the Itô form of (2.14):

$$(5.1) \qquad 2\mathrm{i}\,(\theta k)\,d_z\psi + \triangle_{\mathbf{x}}\psi\,dz + \frac{\mathrm{i}(\theta^3 k^3)\delta^2}{4}R_0(0)\psi\,dz + (\theta^2 k^2)\delta\psi d_z B\left(z,\frac{\mathbf{x}}{\delta}\right) = 0\,,$$

with the law of the Brownian flow ∇B coinciding with the law of the flow $\mathbf{B}$ in (2.17). This Itô form of the Schrödinger equation is discussed in, for instance, [11]. Now different regimes lead to different Wigner distributions and equations that they satisfy, and, hence, different Green's functions, which shape the Green's function filter.

5.1. Subsequent high-frequency scaling. First, we consider the situation with a subsequent high-frequency or geometrical optics limit followed by the large diversity scaling. That is, we have

$$(5.2) \qquad \varepsilon \ll \frac{1}{\theta} \ll \delta \ll 1\,.$$

In this case, the Wigner distribution in (2.16) again satisfies (2.20)! Therefore, the Green's function estimation corresponds to the estimation discussed above.

5.2. The joint limit. We discuss next the joint limit with θ and δ going to zero simultaneously, that is,

$$(5.3) \qquad \varepsilon \ll \frac{\xi}{\theta} = \delta \ll 1$$

for $\xi = \mathcal{O}(1)$. As shown in [34], the Wigner distribution in (2.16) converges in the limit $\delta = \xi\theta \to 0$ weakly (in $\mathcal{S}'(\mathbb{R}^{2d})$) and in probability to $\widetilde{W}$, solving

$$(5.4) \qquad \frac{\partial \widetilde{W}}{\partial z}(z,\mathbf{x},\mathbf{p}) + \frac{\mathbf{p}}{\omega}\cdot\nabla_{\mathbf{x}}\widetilde{W}(z,\mathbf{x},\mathbf{p})$$
$$= \frac{\omega^2\xi^2}{4}\iint_{-\infty}^{\infty}\frac{d\mathbf{q}}{(2\pi)^d}\widehat{R}_0(\mathbf{q})\left(\widetilde{W}(z,\mathbf{x},\mathbf{p}+\mathbf{q}) - \widetilde{W}(z,\mathbf{x},\mathbf{p})\right)$$

(cf. (2.19) for the definition of R_0). The Green's function of (5.4) is explicitly given by

$$\widetilde{U}(z,\mathbf{x},\mathbf{p};\mathbf{x}^0,\mathbf{p}^0) = \iint_{-\infty}^{\infty}\frac{1}{\omega^d(2\pi)^{2d}}\exp\left(\mathrm{i}\mathbf{w}\cdot(\mathbf{x}-\mathbf{x}^0) + \mathrm{i}\mathbf{r}\cdot\frac{(\mathbf{p}-\mathbf{p}^0)}{\omega} - \mathrm{i}z\mathbf{w}\cdot\frac{\mathbf{p}^0}{\omega}\right)$$
$$(5.5) \qquad \times \exp\left(-\frac{\omega^2\xi^2}{4}\int_0^z D_R\left(\frac{\mathbf{r}+\mathbf{w}s}{\omega}\right)ds\right)d\mathbf{w}\,d\mathbf{r}$$

and replaces U in (2.21). Here, D_R is the medium structure function,

$$(5.6) \qquad\qquad D_R(\mathbf{r}) = R_0(\mathbf{0}) - R_0(\mathbf{r});$$

cf. (2.19). The expression (3.18) for the Green's function filter then becomes

$$(5.7) \quad \widetilde{\check{\Lambda}}(z, \omega, \mathbf{x}, \mathbf{y}; \sigma_t, \sigma_x)$$

$$\approx \iint_{-\infty}^{\infty} \frac{e^{-i\mathbf{p}\cdot\mathbf{y}}}{(2\pi)^{2d}} \exp\left(i\mathbf{w}\cdot(\mathbf{x}-\mathbf{x}^0) + i\mathbf{r}\cdot\frac{(\mathbf{p}-\mathbf{p}^0)}{\omega} - iz\mathbf{w}\cdot\frac{\mathbf{p}^0}{\omega} \right)$$

$$\times \exp\left(-\frac{\omega^2\xi^2}{4} \int_0^z D_R\left(\frac{\mathbf{r}+s\mathbf{w}}{\omega}\right) ds \right)$$

$$\times \widehat{C}_0(\omega, \mathbf{p}_0) \frac{\chi^2\left(\frac{\mathbf{x}_0-\mathbf{x}_c}{A}\right)}{(2\pi)^d} \left(\frac{1}{\omega}\right)^d dw\, dr\, dp\, dx_0\, dp_0$$

$$= \frac{1}{(4\pi)^d} \iint e^{i\omega\mathbf{w}\cdot(\mathbf{x}-\mathbf{x}_c)} \check{C}_0(\omega, \mathbf{y}+z\mathbf{w}) e^{-\frac{\omega^2\xi^2}{4}\int_0^z D_R(\mathbf{y}+s\mathbf{w})\, ds} \widehat{\chi}_A(\omega\mathbf{w})\, \omega^d\, d\mathbf{w}.$$

In the case where the correlation length associated with the structure function D_R is large, we can expand this, assumed smooth, function D_R,

$$D_R(\mathbf{y}) \mapsto 2D|\mathbf{y}|^2,$$

and recover (3.18). In the joint scaling limit, however, the whole spectrum of the medium fluctuations is involved in the definition of the Green's function filter.

5.3. Long-range media. We finally comment on the situation with rough and long-range media as, for instance, in the turbulent atmosphere and heterogeneous regions of the earth's crust. Here we will consider a white noise limit, however, with the Fresnel number and lateral diversity scales fixed. In this scaling, which is analyzed in detail by Fannjiang and Solna [19, 20, 21], (2.14) becomes

$$(5.8) \qquad\qquad 2i\,(\theta k)\frac{\partial\psi}{\partial z} + \triangle_{\mathbf{x}}\psi + \frac{1}{\sqrt{\varepsilon}}\left(\theta^2 k^2\right) \widetilde{\mu}\left(\frac{z}{\varepsilon}, \mathbf{x}\right)\psi = 0,$$

where the power spectrum of the random field, $\widetilde{\mu}(\cdot, \cdot)$, is given by

$$(5.9) \qquad\qquad \Phi(\vec{\mathbf{k}}) \approx \sigma_H |\vec{\mathbf{k}}|^{-1-2H} |\vec{\mathbf{k}}|^{-d},$$

for $|\vec{\mathbf{k}}|$ in the inertial range, where $\vec{\mathbf{k}} \in \mathbb{R}^{d+1}$ is the spectral variable and H the Hurst exponent characterizing the roughness of the medium fluctuations. That is, we assume that the medium fluctuations follow a power law form over a set of scales called the intertial range, which corresponds to turbulent or long-range medium modeling. In this case, the Wigner distribution solves, in the white noise limit, in the sense of L^2-weak solutions, a Wigner–Itô equation driven by an operator-valued Brownian motion. In particular, the first moment in (2.20) now becomes

$$(5.10) \qquad\qquad \frac{\partial\overline{W}}{\partial z} + \frac{1}{\omega}\mathbf{p}\cdot\nabla_{\mathbf{x}}\overline{W} = \mathcal{Q}_0\overline{W},$$

with

$$\mathcal{Q}_0\overline{W} = \frac{\theta^2\omega^2}{4} \int \Phi(0, \mathbf{q}) \left(-2\overline{W}(\mathbf{p}) + \overline{W}\left(\mathbf{p}+\frac{\mathbf{q}}{\theta}\right) + \overline{W}\left(\mathbf{p}-\frac{\mathbf{q}}{\theta}\right) \right) d\mathbf{q};$$

see [20] for details. The Green's function of (5.10) is

$$\widetilde{U}_\theta(z,\mathbf{x},\mathbf{p};\mathbf{x}^0,\mathbf{p}^0) = \iint_{-\infty}^{\infty} \frac{1}{\omega^d(2\pi)^{2d}} \exp\left(i\mathbf{w}\cdot(\mathbf{x}-\mathbf{x}^0) + i\mathbf{r}\cdot\frac{(\mathbf{p}-\mathbf{p}^0)}{\omega} - iz\mathbf{w}\cdot\frac{\mathbf{p}^0}{\omega}\right)$$

$$(5.11) \qquad \times \exp\left(-\frac{\omega^2\theta^2}{2}\int_0^z D_*\left(\frac{\mathbf{r}+\mathbf{w}s}{\theta\omega}\right)\right) d\mathbf{w}\,d\mathbf{r}\,,$$

corresponding to the form (5.5). The structure function can now be expressed as

$$(5.12) \qquad\qquad D_*(\mathbf{x}) = \int \Phi(0,\mathbf{q})\left(1-e^{i\mathbf{x}\cdot\mathbf{q}}\right) d\mathbf{q}\,.$$

The Green's function filter is therefore again characterized by (5.7). For the power law medium we have the short distance asymptotic

$$(5.13) \qquad\qquad D_*(\mathbf{x}) \approx C_*^2 |\mathbf{x}|^{2H_*}\,,$$

where the effective Hölder exponent H_* is given by

$$(5.14) \qquad\qquad H_* = \begin{cases} H + 1/2 & \text{for } H \in (0,1/2), \\ 1 & \text{for } H \in (1/2,1]\,, \end{cases}$$

in which H is the Hölder exponent of the original medium and C_*^2 a structure parameter.

Note that the effective Hölder exponent H_* is always bigger than $1/2$, corresponding to a "persistent" or a long-range power law. Using this asymptotic and considering a regime with relatively narrow support for the impinging noise field by setting

$$\check{C}_0\left(\sigma_t\omega,\mathbf{y}\right) \mapsto \widehat{f}_0(\omega)\delta(\mathbf{y})\,,$$

we find

$$\check{\Lambda}_H(z,\omega,\mathbf{x},\mathbf{y}) \approx \frac{\omega^d}{(4\pi z)^d}e^{-i\omega\mathbf{y}\cdot\mathbf{x}/z}\widehat{\chi}_A\left(\frac{-\omega\mathbf{y}}{z}\right)\widehat{f}_0(\omega)^* e^{-\frac{(\omega^2\theta^{2-2H_*}z|\mathbf{y}|^{2H_*})C_*^2}{2(2H_*+1)}}\,.$$

For the normalized noise field supported at the carrier frequency ω_c as in (3.22) we thus find that for a fixed Fresnel number the spatial support of the Green's function filter scales as ω_c^{-1/H_*}. That is, the resolution depends *nonlinearly* on the wavelength associated with the characteristic temporal scale of the impinging noise field. In the limit of rough media with $H_* \to 0$ the lateral spatial support of the Green's function filter scales like λ_c^2.

5.4. Applications. Here, we address the application of our analysis to passive seismic tomography, making use of continuous recordings in an array of detectors or receivers. We discuss which scaling regime would apply to the regional study in Southeastern Tibet [43]. In the latter study, the focus was on the "generation" of surface waves. Here, we seek insight into the behavior of body-wave contributions for future applications in the same region. Our analysis incorporates what seismologists refer to as "ambient noise" (our random source distribution) and "coda waves" (through random medium fluctuations).

Concerning the Southeastern Tibet data set discussed in section 1, we obtain the following characterization [43]. The characteristic distance between individual

stations (receivers) is approximately $\mathcal{O}(100\text{km})$, and, similarly, the characteristic transversal distance between passive sources (magnitude $Mw > 5$) is $\mathcal{O}(100\text{km})$. (For smaller earthquakes—but with magnitude $Mw > 4$—the characteristic transversal distance reduces to $\mathcal{O}(10\text{km})$.) The distance from the array to the sources is $\mathcal{O}(5000\text{km})$; most of the sources are likely to be located in the Western Pacific margins and Eastern Indian Ocean margins. The dominant wavelength for shear (S) waves is $\mathcal{O}(20\text{km})$, while the dominant wavelength for compressional (P) waves is $\mathcal{O}(5\text{km})$. (Under certain simplifying conditions, shear waves have been modeled by a scalar wave equation, whence the current analysis would still be applicable.) The correlation length of medium fluctuations is, with the present knowledge, hard to estimate, but a value of $\mathcal{O}(10\text{km})$ is plausible, also, given the complexity in tectonics of the region. The "asymmetry" observed in the cross-correlations in [43] is explained and inherent in our setup based on the paraxial wave equation.

In our modeling, the characteristic transversal distance between stations or sources roughly corresponds to l_x, the distance from the array to the sources roughly corresponds to l_z, and the correlation length of medium fluctuations to l; the dominant wavelength is λ_0. For compressional body waves this results in $\delta \approx 10^{-1}$, $\varepsilon \approx 2 \times 10^{-3}$, and $\theta^{-1} \approx 4 \times 10^{-1}$, thus, corresponding most closely to the scaling discussed in section 5.2.

6. Numerical illustrations. In this section we present a numerical illustration where we show the effect of the Green's function filter. We shall use the filter corresponding to the scaling regime discussed in section 3.3.

We assume that the medium is homogeneous for $z > z_1$ and plot the quantity

$$\mathcal{I}(\tau, \mathbf{x}_1; A, A_D) = \iint G_\theta\left(\tau - s, z_2, \mathbf{x}_2; z_2 - z_1, \mathbf{x}_1 - \frac{\mathbf{y}}{\theta}\right) \Lambda(z_1, s, \mathbf{x}_1, \mathbf{y}) \, ds \, d\mathbf{y},$$

using the approximation in (3.21) for the filter and where we introduce

$$A_D = \sqrt{A^2 + \frac{2D}{3}}.$$

We choose $d = 2$, and in the nondimensionalized coordinates we let

(6.1) $$f_0(t) = e^{-\frac{t^2 \mathcal{D}}{2}} \cos(f_c t),$$

with $\mathcal{D} = 5$, and moreover choose

$$z_1 = 1, \quad \mathbf{x}_c = \mathbf{x}_2 = \mathbf{0}, \quad f_c = 30, \quad \sigma_x = 1.$$

In Figure 6.1, we plot $\mathcal{I}$ in the case with a homogeneous medium. We use the parameter values $A = A_D = 20$ in the left plot. The estimation then captures the wavefield and wavefront for relatively large lateral offsets for the Green's function. The right plot corresponds to the situation with a small aperture, $A = A_D = 1.5$, in which case the wavefield and corresponding "moveout" are not captured.

In Figure 6.2 we plot $\mathcal{I}$ in the case with a random medium. We use the parameter values $A = 1.5, A_D = 9.3$. We then recapture a large part of the wavefield and wavefront (following a hyperbolic "moveout").
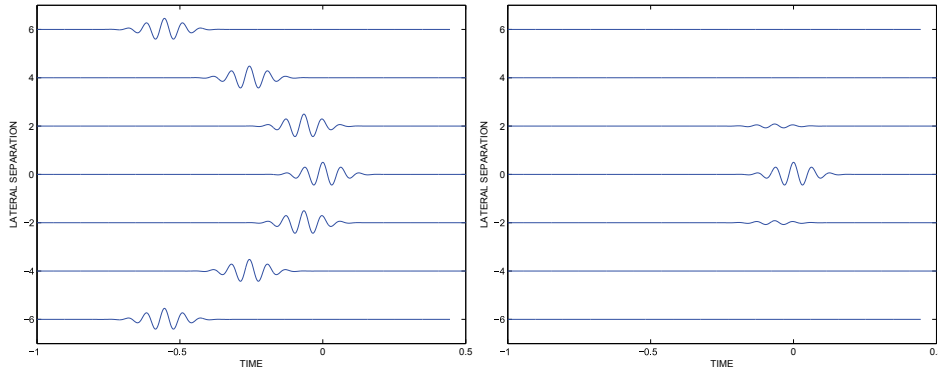
FIG. 6.1. *The normal moveout for a homogeneous medium and large (left) or small (right) aperture.*
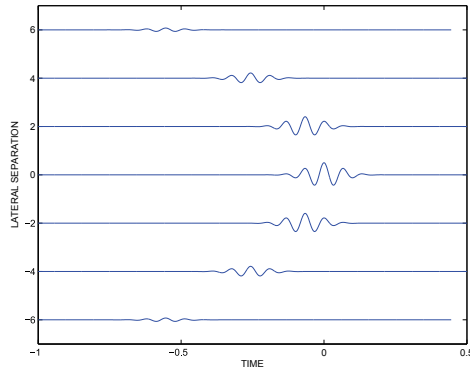

FIG. 6.2. *The normal moveout for a random medium with relatively large effective aperture.*

7. Conclusions. Pairwise cross-correlations between receivers forming arrays provide invaluable data sets where (deterministic) sources (earthquakes) are necessarily absent. The data sets are used to carry out tomography, or inverse scattering, to reveal the properties of the medium away from (below) the array. We tailored a scaling regime to applications in global earth seismology, generating "empirical" Green's functions and "virtual" source experiments. Characterization and knowledge about the structure of the incoherent waves and their correlations is crucial in this context. We have presented a first analysis of this approach to data acquisition in the framework of the paraxial wave approximation in a random medium. The analysis exploits the connection between cross-correlations and time-reversal. The connection is direct in the sense that the Green's function estimation problem can be articulated as the dual of time-reversal superresolution.

Important questions remain, for instance, how to design "optimal" filters, that is, how to combine optimally data in space and frequency to obtain stable and high-resolution estimates so that the filter Λ in (3.19) is near the identity, while enforcing statistical stability.

Appendix. Elements of the proof of Proposition 2.2. Consider the quantity

$$I_\delta(z, \mathbf{x}, \mathbf{y}) = \iint W_\delta(z, \mathbf{x}, \mathbf{p}) e^{-i\mathbf{p}\cdot\mathbf{y}} \, d\mathbf{p} \, .$$

The initial condition in (3.17),

$$W_\delta(0, \mathbf{x}, \mathbf{p}) = W_I(\mathbf{x}, \mathbf{p}),$$

is assumed to be uniformly bounded, Lipschitz continuous, and positive. As explained in [33] we can then write

$$W_\delta(z, \mathbf{x}, \mathbf{p}) = W_I(\mathbf{X}_\delta(z, \mathbf{x}, \mathbf{p}), \mathbf{P}_\delta(z, \mathbf{x}, \mathbf{p})),$$

for the stochastic flow $(\mathbf{X}, \mathbf{P})$ satisfying

$$d\mathbf{X}_z = -\frac{1}{k}\mathbf{P}\,dz, \quad d\mathbf{P}_z = -\frac{k}{2}d\mathbf{B}(z), \quad \mathbf{X}_0 = \mathbf{x}, \quad \mathbf{P}_0 = \mathbf{p}.$$

Observe first that

$$\iint \mathbb{E}\{W_\delta(z, \mathbf{x}, \mathbf{p})\}\, e^{-i\mathbf{p}\cdot\mathbf{y}}\, d\mathbf{p} = \iint \mathbb{E}\{W_I(\mathbf{X}_\delta(z, \mathbf{x}, \mathbf{p}), \mathbf{P}_\delta(z, \mathbf{x}, \mathbf{p}))\}\, e^{-i\mathbf{p}\cdot\mathbf{y}}\, d\mathbf{p}$$

is finite and independent of δ by (2.21). Writing the complex exponential in terms of its real and imaginary parts and decomposing the domain of integration for the corresponding integrals into subsets where $\cos(\mathbf{p}\cdot\mathbf{y})$ (respectively, $\sin(\mathbf{p}\cdot\mathbf{y})$) is positive (respectively, negative), we can apply Tonelli's theorem and interchange the order of integration and expectation and get

$$(A.1) \qquad \mathbb{E}\{I_\delta(z, \mathbf{x}, \mathbf{y})\} = \iint \mathbb{E}\{W_\delta(z, \mathbf{x}, \mathbf{p})\}\, e^{-i\mathbf{p}\cdot\mathbf{y}}\, d\mathbf{p};$$

thus, $I_\delta(z, \mathbf{x}, \mathbf{y})$ is finite with probability one, and its expectation given by (A.1).

By a corresponding application of Tonelli's theorem we can write

$$\mathbb{E}\{I_\delta^2(z, \mathbf{x}, \mathbf{y})\} = \iint \mathbb{E}\{W_\delta(z, \mathbf{x}, \mathbf{p}_1)W_\delta(z, \mathbf{x}, \mathbf{p}_2)\}\, e^{-i(\mathbf{p}_1+\mathbf{p}_2)\cdot\mathbf{y}}\, d\mathbf{p}_1\, d\mathbf{p}_2\,.$$

In [33] it is shown that $\mathbb{E}\{W_\delta^2(z, \mathbf{x}, \mathbf{p})\}$ is integrable in $\mathbf{p}$, and that

$$\lim_{\delta\to 0} \mathbb{E}\{W_\delta(z, \mathbf{x}, \mathbf{p}_1)W_\delta(z, \mathbf{x}, \mathbf{p}_2)\} = \mathbb{E}\{W_\delta(z, \mathbf{x}, \mathbf{p}_1)\}\,\mathbb{E}\{W_\delta(z, \mathbf{x}, \mathbf{p}_2)\}\,.$$

By the Lebesgue dominated convergence theorem we can therefore conclude that

$$\lim_{\delta\to 0} \mathbb{E}\{I_\delta^2(z, \mathbf{x}, \mathbf{y})\} = \mathbb{E}^2\{I_\delta(z, \mathbf{x}, \mathbf{y})\}\,.$$

REFERENCES

[1] D. V. ALFARO AND K. SOLNA, *Time-Reversal for Inclusion Detection in Randomly Layered Media*, submitted, 2008.

[2] G. BAL, G. PAPANICOLAOU, AND L. RYZHIK, *Radiative transport limit for the Schrödinger equation*, Nonlinearity, 15 (2002), pp. 513–529.

[3] C. BARDOS, J. GARNIER, AND G. PAPANICOALOU, *Identification of Green's function singularities by cross correlation of noisy signals*, Inverse Problems, 24 (2008), paper 015011.

[4] P. BLOMGREN, G. PAPANICOLAOU, AND H. ZHAO, *Super-resolution in time-reversal acoustics*, J. Acoust. Soc. Amer., 111 (2002), pp. 230–248.

[5] L. BORCEA, G. PAPANICOLAOU, AND C. TSOGKA, *Asymptotics for the space-time Wigner transform with applications to imaging*, in Stochastic Differential Equations: Theory and Applications, P. H. Baxendale and S. V. Lototsky, eds., Interdiscip. Math. Sci. 2, World Scientific, River Edge, NJ, 2007, pp. 91–112.

[6] L. BORCEA, G. PAPANICOLAOU, AND C. TSOGKA, *Coherent interferometric imaging*, Geophysics, 71 (2006), pp. S1165–S1175.

[7] M. CAMPILLO AND A. PAUL, *Long-range correlations in the diffuse seismic coda*, Science, 299 (2003), pp. 547–549.

[8] J. F. CLAERBOUT, *Synthesis of a layered medium from its acoustic transmission response*, Geophysics, 33 (1968), pp. 264–269.

[9] J. F. CLAERBOUT, *Coarse grid calculations of waves in inhomogeneous media with application to delineation of complicated seismic structure*, Geophysics, 35 (1970), pp. 407–418.

[10] Y. COLIN DE VERDIÈRE, *Mathematical Models for Passive Imaging* I: *General Background*, preprint, 2006; available online at http://www-fourier.ujf-grenoble.fr/ycolver/Sismo/big1.pdf.

[11] D. DAWSON AND G. PAPANICOLAOU, *A random wave process*, Appl. Math. Optim., 12 (1984), pp. 97–114.

[12] M. V. DE HOOP AND A. T. DE HOOP, *Wave-field reciprocity and optimization in remote sensing*, Proc. R. Soc. Lond. A., 456 (2000), pp. 641–682.

[13] A. DERODE AND M. FINK, *How to estimate the Green's function of a heterogeneous medium between two passive sensors? Application to acoustic waves*, Appl. Phys. Lett., 83 (2003), pp. 3054–3056.

[14] A. DERODE, E. LAROSE, M. TANTER, J. DE ROSNY, A. TOURIN, M. CAMPILLO, AND M. FINK, *Recovering the Green's function from field-field correlations in an open scattering medium*, J. Acoust. Soc. Amer., 113 (2003), pp. 2973–2976.

[15] D. DRAGANOV, K. WAPENAAR, W. MULDER, J. SINGER, AND A. VERDEL, *Retrieval of reflections from seismic background-noise measurements*, Geophys. Res. Lett., 34 (2007), paper L04305; doi:10.1029/2006GL028735.

[16] T. L. DUVALL, S. M. JEFFERIES, J. W. HARVEY, AND A. POMERANTZ, *Time distance helioseismology*, Nature, 362 (1993), pp. 430–432.

[17] A. FANNJIANG, *White-noise and geometrical optics limits of Wigner–Moyal equation for beam waves in turbulent media*. II. *Two-frequency formulation*, J. Statist. Phys., 120 (2005), pp. 543–586.

[18] A. FANNJIANG, *Two-frequency radiative transfer and asymptotic solution*, J. Opt. Soc. Amer. A, 24 (2007), pp. 2248–2256.

[19] A. FANNJIANG AND K. SOLNA, *Scaling limits for laser beam propagation in atmospheric turbulence*, Stoch. Dyn., 4 (2004), pp. 135–150.

[20] A. C. FANNJIANG AND K. SOLNA, *Propagation and time reversal of wave beams in atmospheric turbulence*, Multiscale Model. Simul., 3 (2005), pp. 522–558.

[21] A. FANNJIANG AND K. SOLNA, *Superresolution and duality for time-reversal of waves in random media*, Phys. Lett. A, 352 (2005), pp. 22–29.

[22] M. FINK, *Time-reversed acoustics*, Scientific American, Nov. (1999), pp. 91–97.

[23] J. P. FOUQUE, J. GARNIER, A. NACHBIN, AND K. SØLNA, *Imaging of a dissipative layer in a random medium using a time reversal method*, in Proceedings of the conference "Monte Carlo and Quasi-Monte Carlo Methods 2004," Nice, 2004, H. Niederreiter and D. Talay, eds., Springer, Berlin, 2005, pp. 127–145.

[24] J. P. FOUQUE, J. GARNIER, A. NACHBIN, AND K. SOLNA, *Time reversal refocusing for point source in randomly layered media*, Wave Motion, 42 (2005), pp. 191–288.

[25] J. P. FOUQUE, J. GARNIER, G. PAPANICOLAOU, AND K. SOLNA, *Wave Propagation and Time Reversal in Randomly Layered Media*, Springer, New York, 2007.

[26] J. GARNIER, *Imaging in randomly layered media by cross-correlating noisy signals*, Multiscale Model. Simul., 4 (2005), pp. 610–640.

[27] P. GERSTOFT, K. G. SABRA, P. ROUX, W. A. KUPERMAN, AND M. C. FEHLER, *Green's function extraction and surface-wave tomography from microseisms in southern California*, Geophysics, 71 (2006), pp. S123–S131.

[28] R. HE, B. E. HORNBY, AND G. SCHUSTER, *3D wave-equation interferometric migration of VSP multiples*, SEG Expanded Abstracts, 25 (2006), 3442.

[29] K. HUANG, G. PAPANICOLAOU, K. SØLNA, C. TSOGKA, AND H. ZHAO, *Efficient numerical simulation for long range wave propagation*, J. Comput. Phys., 215 (2006), pp. 448–464.

[30] W. A. KUPERMAN, W. S. HODGKISS, H. C. SONG, T. AKAL, C. FERLA, AND D. R. JACKSON, *Phase conjugation in the ocean: Experimental demonstration of an acoustic time-reversal mirror*, J. Acoust. Soc. Amer., 103 (1997), pp. 25–40.

[31] G. Lerosey, J. de Rosny, A. Tourin, A. Derode, and M. Fink, *Time reversal of wideband microwaves*, Appl. Phys. Lett., 88 (2006), paper 154101.

[32] M. Levy, *Parabolic Equation Methods for Electromagnetic Wave Propagation*, The Institution of Electrical Engineers, Herts, UK, 2000.

[33] G. Papanicolaou, L. Ryzhik, and K. Sølna, *Statistical stability in time reversal*, SIAM J. Appl. Math., 64 (2004), pp. 1133–1155.

[34] G. Papanicolaou, L. Ryzhik, and K. Sølna, *Self-averaging from lateral diversity in the Itô–Schrödinger equation*, Multiscale Model. Simul., 6 (2007), pp. 468–492.

[35] P. Roux, K. G. Sabra, P. Gerstoft, W. A. Kuperman, and M. Fehler, *P-waves from cross correlation of seismic noise*, Geophys. Res. Lett., 32 (2005), paper L19303; doi:10.1029/2005GL023803.

[36] K. Sabra, P. Roux, and W. A. Kuperman, *Arrival-time structure of the time averaged ambient noise cross-correlation function in an ocean waveguide*, J. Acoust. Soc. Amer., 117 (2005), pp. 164–174.

[37] F. Scherbaum, *Seismic imaging of the site response using micro-earthquake recordings. Part II: Application to the Swabian Jura, Southwest Germany, seismic network*, Bull. Seismol. Soc. Am., 77 (1987), pp. 1924–1944.

[38] N. M. Shapiro and M. Campillo, *Emergence of broadband Rayleigh waves from correlations of the ambient seismic noise*, Geophys. Res. Lett., 31 (2004), paper L07614.

[39] N. M. Shapiro, M. Campillo, L. Stehly, and M. Ritzwoller, *High-resolution surface-wave tomography from ambient seismic noise*, Science, 307 (2005), pp. 1615–1618.

[40] K. Sølna and G. C. Papanicolaou, *Ray theory for a locally layered medium*, Waves in Random Media, 10 (2000), pp. 151–198.

[41] F. D. Tappert, *The parabolic approximation method*, in Wave Propagation and Underwater Acoustics, Lecture Notes in Phys. 70, Springer-Verlag, Berlin, 1977.

[42] B. A. van Tiggelen, *Green function retrieval and time reversal in a disordered world*, Phys. Rev. Lett., 91 (2003), paper 243904.

[43] H. Yao, R. D. van der Hilst, and M. V. de Hoop, *Surface-wave array tomography in SE Tibet from ambient seismic noise and two-station analysis—I. Phase velocity maps*, Geophys. J. Int., 166 (2006), pp. 732–744.

[44] J. Yu and G. T. Schuster, *Crosscorrelogram migration of inverse vertical seismic profile data*, Geophysics, 71 (2006), pp. S1–S11.

[45] K. Wapenaar, J. Fokkema, and R. Snieder, *Retrieving the Green's function in an open system by cross correlation: A comparison of approaches (L)*, J. Acoust. Soc. Amer., 118 (2005), pp. 2783–2786.

[46] R. L. Weaver and O. I. Lobkis, *Ultrasonics without a source: Thermal fluctuation correlations at Mhz frequencies*, Phys. Rev. Lett., 93 (2001), paper 254301.

[47] M. E. Willis, R. Lu, X. Campman, M. N. Toksöz, Y. Zhang, and M. V. de Hoop, *A novel application of time-reversed acoustics: Salt-dome flank imaging using walkaway VSP surveys*, Geophysics, 71 (2006), A7–A11.